2022

Gravity Dependence Quantifiers for Vapor Compression Cycles Subjected to Inclination Testing and Parabolic Flights

Leon Philipp Martin Brendel

Stephen L. Caskey

James E. Braun

Eckhard A. Groll

Gravity Dependence Quantifiers for Vapor Compression Cycles Subjected to Inclination Testing and Parabolic Flights

Leon P. M. BRENDEL[1]*, Stephen L. CASKEY[2], James E. BRAUN[1], Eckhard A. GROLL[1]

[1]Ray W. Herrick Laboratories, School of Mechanical Engineering, Purdue University
West Lafayette, 47907-2099, IN, USA

[2]Air Squared, Inc. 675 E 124th Ave, Thornton, CO 80241, USA

*brendel@purdue.edu

ABSTRACT

Increased utilization of vapor compression cycles for spacecraft is foreseen due to the relatively high COPs compared to alternative technologies for food refrigeration and air-conditioning. However, system level publications about effects of microgravity on a vapor compression cycle are still very scarce. Over the course of a NASA Small Business Innovation Research project, data was collected from one vapor compression cycle that was exposed to both inclination testing on-ground and microgravity maneuvers in-flight while operating continuously. Different quantifiers were introduced and developed to compare seven datasets differentiated by the type of gravity perturbations and refrigerant. All gravity perturbations affected the measurements, but the responses were often difficult to classify, let alone quantify. The most useful quantifier identified was the MIN/MAX-measure, capturing the span of values measured due to a gravity perturbation (maximum minus minimum). This quantifier identified a decreasing gravity dependence as a function of increasing mass flux across all datasets. Depending on the cycle mass flux, gravity induced changes of the evaporation temperature were in a range of 1 to 10 K, whereas the evaporator heat transfer rate varied by up to +/-50% and as little as +/-2%. Generally, the collected datasets show inclination changes cause stronger cycle responses than parabolic flight maneuvers.

Keywords: Vapor compression cycle, inclination testing, parabolic flights, gravity, two-phase, refrigeration, food storage

1. INTRODUCTION

Vapor compression cycles have been proposed for space applications recurrently over the last several decades (Chiaramonte and Joshi, 2004; Ginwala, 1961; Hye, 1985). However, confidence in application of the technology in microgravity is still low. A thorough introduction to the topic can be found in Brendel et al. (2021). Detailed studies about the effects of gravity exist mainly for two-phase flow fundamentals like the condensation or evaporation heat transfer coefficient (Azzolin et al., 2018; Iceri et al., 2020; Narcy, 2014). A frequent finding was that effects of gravity changes decrease as the flow velocities increase. System level studies were usually not sufficiently documented to provide strong conclusions (Domitrovic et al., 2003; Grzyll and Cole, 2000; Sunada et al., 2008).

Rohleder et al. (2018) initiated an SBIR project which dedicated significant resources to testing a vapor compression cycle both at varying orientations on the ground as well as during parabolic flights. Cycle instabilities induced by gravity perturbations were one core interest that was evaluated with differently developed quantifiers. Several results have already been published. This study summarizes all testing series collected and presents the application of different gravity dependence quantifiers. General findings are derived from the large comparison made while highlighting the advantages and caveats of the quantifiers.

2. METHODOLOGY

2.1 Test setup

The test stand is described in several journal publications and a PhD thesis (Brendel, 2021). Therefore, it is only introduced at a high level for this paper.

The refrigeration cycle was a simple, four-component vapor compression cycle with secondary loops as a heat source and sink. Initially, water was used as both, the heat source and sink, where the heat exchangers were of helical coil tube-in-tube type. Later, fin-tube heat exchangers were implemented to capture any differences on system operation with different heat exchanger types and secondary loop working fluids., The heat source was a closed air loop with an electric heater to maintain a desired temperature and the heat sink was ambient air, dependent on the environmental conditions where the test stand was operating. Figure 1 shows a schematic of the cycle in the air-to-air configuration. Temperature and pressure measurements were installed at the inlet and outlet of each of the four components and Coriolis-type mass flow meters were installed in both the liquid line and the suction line. The entire test stand could be inclined to a specific angle to change the direction of the gravity vector imposed on the operation of the cycle. The experimental apparatus was used for several different test series, which are differentiated by three main categories: the gravity perturbation pattern (on-ground inclination versus in-flight parabolic maneuvers), the test stand configuration (water-to-water versus air-to-air), and the refrigerant type (R134a versus R1234ze(E)).

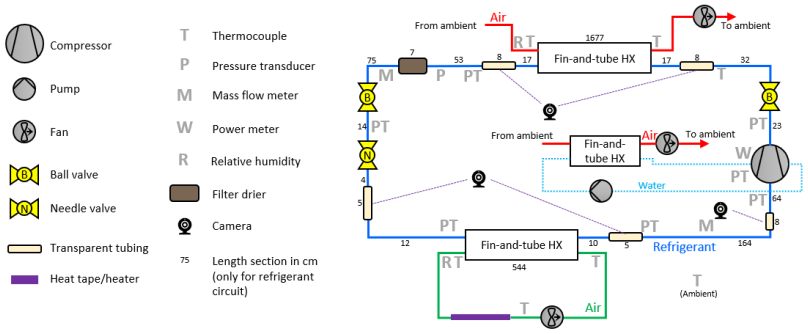

Figure 1: Schematic of refrigeration cycle test stand in air-to-air configuration.

2.2 Gravity perturbation patterns

A *gravity perturbation* is either a change of the inclination angle or a change of the gravitational acceleration. A gravity perturbation *pattern* is a sequence of gravity perturbations which is repeated at varying operating conditions in the experiments. Four gravity perturbation patterns are distinguished and illustrated in both Table 1 and Figure 2. The imposed rate of angle changes "slow", "medium" and "fast" are only meaningful relative to each other:

- Steady-state testing (slow angle changes)
  - The inclination angle changed in increments of 45°. Inclination angles were locked until the cycle reached steady-state (Brendel et al., 2022a). This resulted in different locked angle times because the cycle needed different durations to reach steady-state.
- 6-angle testing (medium pace angle changes)
  - The inclination angle was changed in increments of 90°and each angle was locked for exactly 2 minutes. The inclination angle pattern was $\theta = \{0°, 90°, +180°, -180°, -90°, 0°\}$
- Parabolic flight simulations (fast pace angle changes)
  - The inclination angle was changed between +90° and -90°. The pattern and timing was derived to mimic expected gravity perturbations during parabolic flight profiles (Brendel et al., 2021a).
- Parabolic flights (fast paced gravity changes)
  - The only gravity perturbation which changed the gravitational force but not its direction. The pattern starts with 1.8 g level and alternates between 0 g for 20 seconds and 1.8 g for 40 seconds until 0 g was established five times. Hyper gravity (1.8 g) and residual gravity (0 to 1 g) during the transitions always acts perpendicular to the tabletop (same direction it would act while on the ground in a horizontal position).

2.3 Available datasets

The four, unique gravity perturbation patterns were executed on different test stand configurations and refrigerants. Overall, seven different datasets listed in Table 2 can be distinguished based on the three characteristics. For the steady-state set, R134a and R1234ze(E) data points are collected in one datasets because the total number of data points is small and the results are very similar. The last column of Table 2 reports the number of completed gravity perturbations executed for each of the datasets. This number does not count test runs removed due to incorrect executions of the inclination changes (angle overshoot or lack of steady-state), undercharged operating conditions (loss of subcooling), malfunctioning data acquisition (missing measurements) and other issues. A detailed listing of removed test runs can be found in Brendel (2021).

Table 1: Sequence of steps for each gravity perturbation captured.

Step	**Steady-state**		**6-angle**		**Simulations**		**Flights**	
	Angle [°]	*Time [s]*	*Angle [°]*	*Time [s]*	*Angle [°]*	*Time [s]*	*Gravity [g_e]*	*Time [s]*
1	0	N/A	0	120	0	5	1.8	~20
2	45	N/A	90	120	90	20	0	~20
3	90	N/A	180	120	-90	20	1.8	~40
4	135	N/A	-180	120	90	40	0	~20
5	180	N/A	-90	120	-90	20	1.8	~40
6	-180	N/A	0	120	90	40	0	~20
7	-135	N/A			-90	20	1.8	~40
8	-90	N/A			90	20	0	~20
9	-45	N/A			0	5	1.8	~40
10	0	N/A					0	~20
11							1.8	~20

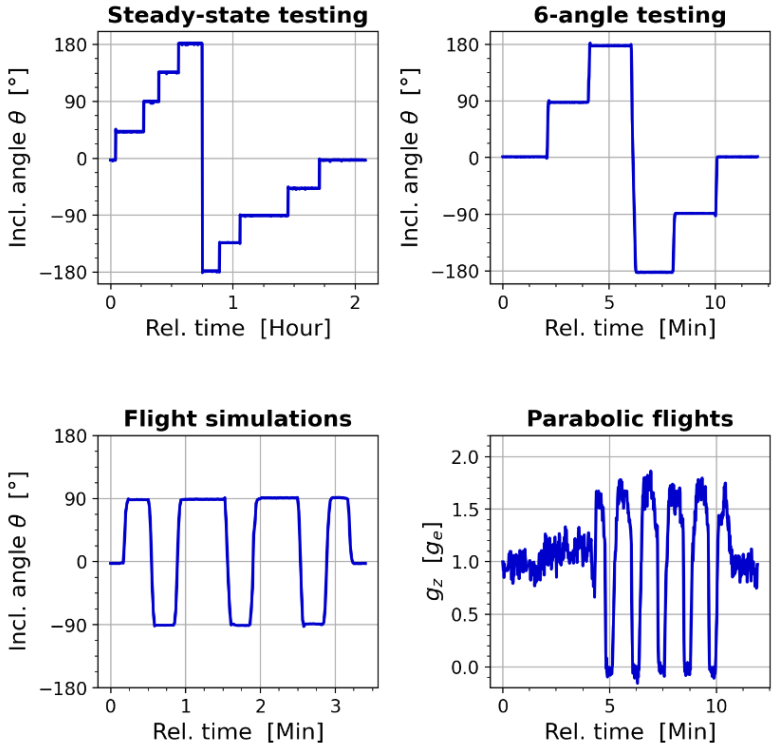

Figure 2: Example measurements plotted from each of the four gravity perturbation patterns.

Table 2: Overview of seven collected datasets across four gravity perturbations, two cycle configurations, and two refrigerants.

Set	*Type*	*Frequency of gravity perturbations*	*Configuration**	*Refrigerants*	*Number of clean test runs*
1	Steady-state	low	AA	R134a+R1234ze(E)	7
2	6-angle	medium	LL	R134a	22
3	6-angle	medium	AA	R134a	31
4	6-angle	medium	AA	R1234ze(E)	11
5	Simulations	fast	AA	R134a	12
6	Simulations	fast	AA	R1234ze(E)	13
7	Parabolic flights	fast	AA	R134a	14
*LL: Liquid-to-liquid; AA: air-to-air					

3. QUANTIFIERS

3.1 Effects of changes of the inclination angle

Gravity perturbation quantifiers were designed by a process of trial and error to characterize the measured system response. The design objectives were a physical meaning or basis, general applicability on a broad range, and utility or usefulness of the quantifier. Figure 3 shows a drawing of a possible cycle response to inclination changes, which helps to understand some caveats associated with the quantifiers. The figure shows a hypothetically response of the cooling capacity but is interchangeable with most other measurements. The response is not specific to a certain gravity perturbation pattern but shows as many relevant and frequently observed phenomena as possible. Although the drawing shown is not from direct measurements, it is realistic based on the experiences of the authors. The thick blue line plotted against the right-hand side y-axis shows a hypothetical inclination pattern. The thick red line plotted against the left-hand side y-axis shows the response of the cooling capacity in Watts. The thin red dash-dotted line reports the initial cooling capacity throughout the entire plot. If the cycle was gravity independent, the thick, solid red line would continue along this horizontal line. The x-axis is divided into sections of approximately 2 minutes as generated in 6-angle testing and sections of approximately 15 minutes which were typical durations in steady-state testing. The numbers, upper-case and lower-case letters in the figure have the following meanings:

- Capital letters show observable phenomena:
    - A. The cycle may spike sharply upon an inclination change.
    - B. Typically, the cycle immediately starts to asymptotically converge to a value between the previous steady-state and the maximum (minimum) value of the spike.
    - C. A new steady-state is sometimes achieved within 2 minutes and usually has a deviation from the initial steady-state value.
    - D. Another change of inclination angle may lead to spikes in the same or the opposite direction of previous spikes. Moreover, the spikes may have a flatter slope or even come with delay.
    - E. The recovery from the spike may happen slowly and the cycle may not have reached a new steady-state after 2 minutes.
    - F. Some changes of the inclination angle may not cause any spike. For small angle changes, it is also possible that the steady-state does not change.
    - G. Some inclination angles can cause fluctuations in the suction line pressure and mass flow rate (Brendel et al., 2022a). Such oscillations were only found in the suction line but not in the liquid line and are probably rooted in the two-phase flow regimes in the evaporator.
    - H. The cycle does not necessarily approach or return to the initial steady-state when at initial inclination angle even after waiting a long time.
- Lower case letters show areas of deviation from the initial steady-state operation
    - a. and c. Integrated cooling energy was less compared to operation without gravity changes.
    - b. Integrated cooling energy was greater compared to operation without gravity changes.
- Numbers show important values for post processing
    1. The initial steady-state measurement.
    2. The minimum measured value through the entire gravity perturbation pattern.
    3. The steady-state value associated with $\theta = +90°$ (or any other angle part of the gravity perturbation procedure)
    4. The maximum measured value through the gravity perturbation pattern.
    5. The steady-state at the given angle (here $\theta = -90°$).
    6. The steady-state at the given angle (here $\theta = -120°$).
    7. The final steady-state at the initial angle.
    8./9. For each transient measurement, an $80^{th}/20^{th}$ percentile can be determined, where points 8 and 9 represent upper and lower cutoffs where 80% of all data points are centered, such that 20% of the data have deviations from the initial value that are outside of the cut offs. A constant sampling rate is applied.

Points 3, 5 and 6 can only be reliably obtained during steady-state testing. For 6-angle testing and flight simulations, the cycle usually did not settle to a new steady-state before the next gravity perturbation took place and can therefore be called “dynamic” testing. Generally speaking, *steady-state* testing captures the entire range of phenomena depicted in Figure 3. Transient data associated with *6-angle* testing typically allows estimation of steady-state behavior for each

position and whether oscillations will occur or not. Transient data from *flight simulations* leads to at least the first peak response, but the next gravity perturbation may be enacted before a clear trend towards a new steady-state is visible. The cycle responses on parabolic flights usually have a different nature as explained in Brendel et al. (2022b).

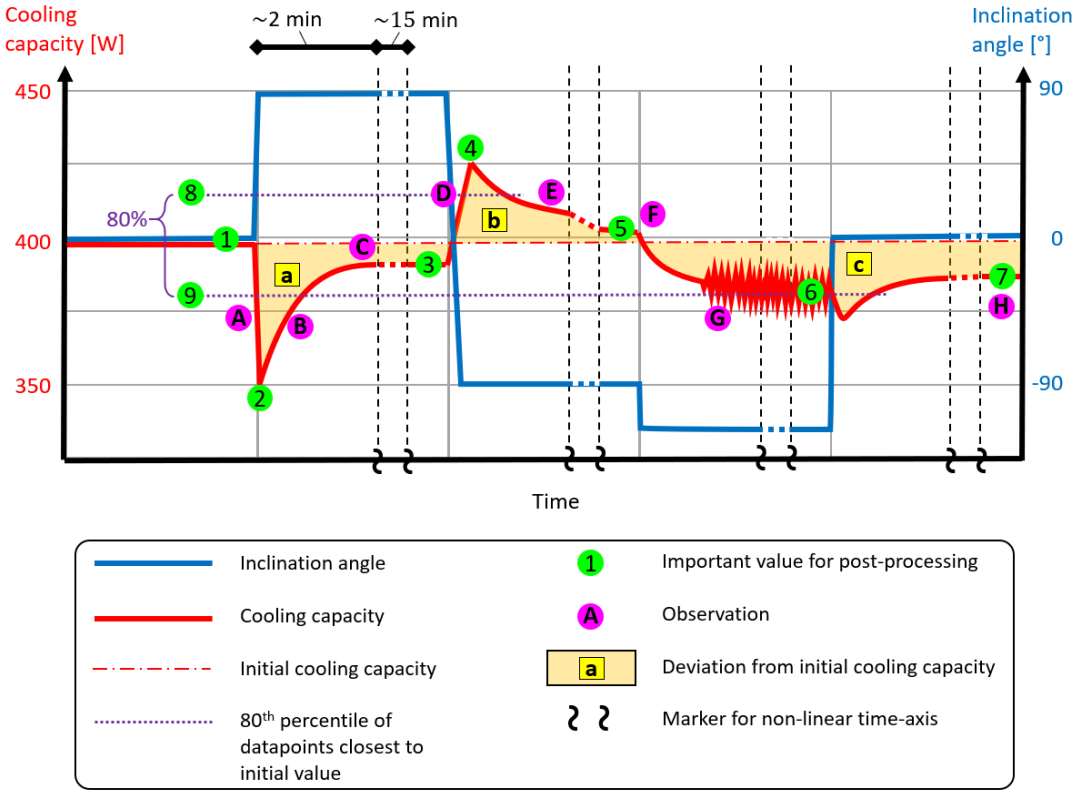

Figure 3: Example cycle responses to inclination angle changes.

3.2 Proposed quantifiers

MDV (Mean deviation)

The mean deviation of a measurement from its initial value can be calculated by summing up the areas "a", "b" and "c" in Figure 3 and dividing them by the elapsed time. However, if "b" was equal to "a+c", then the mean deviation would misleadingly be 0. Therefore, the absolute values of "a", "b" and "c" are summed up. Hence, for any measurement x, the MDV is calculated as in Equation 1 and has the units of x:

$$MDV = \frac{\int_{t_{start}}^{t_{end}} |x(t) - x(0)|\, dt}{t_{end} - t_{start}}, \tag{1}$$

The equation immediately shows a twofold dependence of the MDV on the timing of the gravity perturbation pattern:

1. The MDV becomes smaller if the initial steady-state is maintained longer relative to the complete pattern (same area a+b+c but larger denominator).
2. If the locking times of the gravity perturbation pattern are short, then the MDV will be primarily affected by the frequently observed spikes and speed of recovery. If the locking times are long, then the MDV will be predominantly affected by the steady-state operation of the respective angles (which is closer to the initial steady-state than the preceding spike and therefore leads to a lower MDV).

The integral form of Equation 1 suggests that the MDV is designed for heat and mass flow rates. However, since the MDV is simply the mean deviation, x can be replaced also with pressures and temperatures. In the presented work, the MDV was rarely directly used as a quantifier but as a vehicle to compute the inclination impact ratio (IIR) defined in the following.

IIR (Inclination impact ratio)

It is useful to express the mean deviation relative to the magnitude of the measurements. The initial steady-state (point 1 in Figure 3) is used as a reference value and the quantifier is expressed as a percentage as defined in Equation 2:

$$IIR = \frac{MDV}{x(0)} \cdot 100\%. \quad (2)$$

The locking time dependence of the MDV also applies to the IIR, since it is directly derived from the MDV.

MMX (Difference between maximum and minimum value)
The MMX is computed by searching for the maximum and minimum measured value of transient data from a test execution (points 2 and 4 in Figure 3). The difference of the two is the MMX defined in Equation 3:

$$MMX = \max\big(x(t)\big) - \min\big(x(t)\big), \text{for all t in } \{t_{start}, t_{end}\} \quad (3)$$

The MMX is mostly independent of the durations of gravity perturbations, because the maximum and minimum values are usually determined by spikes shortly after gravity perturbations. A drawback of the MMX is that a brief spike increases the MMX although it might be dampened by thermal masses and not meaningful for some applications. Additionally, the MMX is very sensitive to short and even random spikes. For example, when the data acquisition system records a single 0 for a random reason, the MMX will immediately be very large. The sensitivity can be reduced with the 80% quantifier.

80% (80% of all data points producing the smallest range of measurements)
The 80% quantifier is closely related to the MMX, but it considers only 80% of the data points collected by one sensor during a gravity perturbation pattern. To compute it, the 80% of data points must be found which result in the smallest range of data. Figure 3 shows dotted lines in purple representing approximate cutoffs. The 80% quantifier is always smaller than the MMX because the largest spikes are shaved off. Instead of 80%, a higher or smaller percentile could be used, depending on how sensitive the quantifier should be to short spikes.

MMX/AVG and 80%/AVG
The MMX and 80% quantifiers can also be expressed as a percentage by dividing them by the initial steady-state value (INI) or by the average of all the transient data points (AVG). For most measurements other than temperature, this is a more meaningful comparison: An MMX of 10 W is significant if the initial cooling capacity is 40 W, but it is insignificant if the initial cooling capacity is 400 W. The expression as a percentage captures this.

4. RESULTS

4.1 IIR

Figure 4 shows the cooling capacity IIR measured on the *refrigerant* side for all datasets organized by the gravity perturbation pattern. A decreasing trend for an increased mass flux is evident for all types of dynamic testing (6-angle, simulations, flights) but not for steady-state testing. Parabolic flight data shows the least pronounced trend due to the significant scatter of the data.

The only IIRs exceeding 10% were measured for the liquid-to-liquid configuration (6-angle testing). It is not clear whether the high gravity dependence was caused by the different evaporator or by the larger inner tube diameter resulting in lower mass fluxes. Regardless of the reason, the liquid-to-liquid and air-to-air data from 6-angle testing form a similar/comparable trend across a wide range of mass fluxes $2.2\ kg/(m^2 \cdot s) < G < 63.6\ kg/(m^2 \cdot s)$. This trend was yet clearer when considering the IIRs calculated for the heat transfer rate of the *heat source* side in steady-state for the refrigerant side (Brendel et al., 2021b).

For all comparisons of R134a and R1234ze(E), the quantifier trends and magnitudes are very similar. This can be directly explained with the similar thermophysical properties of both refrigerants but reaching a good agreement was not clear a priori.

The major outlier among the datasets is the steady-state testing results shown in Figure 4. While IIR results from *dynamic testing* ranged between 1 and 8% for the air-to-air configuration, the *steady-state* testing resulted in a constant $IIR \approx 3\%$ for the mass fluxes 14, 28 and 58 kg/m^2·s. This is most likely explained with the time-dependence

highlighted in section 3.2. With the long locking times of inclination angles, the spikes lost weight in the calculation of the MDV. Instead, the steady-state values dictated the IIR for these tests.

This finding adds to the long-lasting discussion of whether high mass fluxes yield increased resilience of two-phase flows and systems to gravity perturbations: For frequent gravity perturbations,

Figure 4 confirms the hypothesis. However, the effect of mass flux on IIR is insignificant for *slow* changes. A constant IIR also means that the MDV increases as a function of the mass fluxes. Brendel et al. (2022a) investigated exclusively the presented steady-state results.

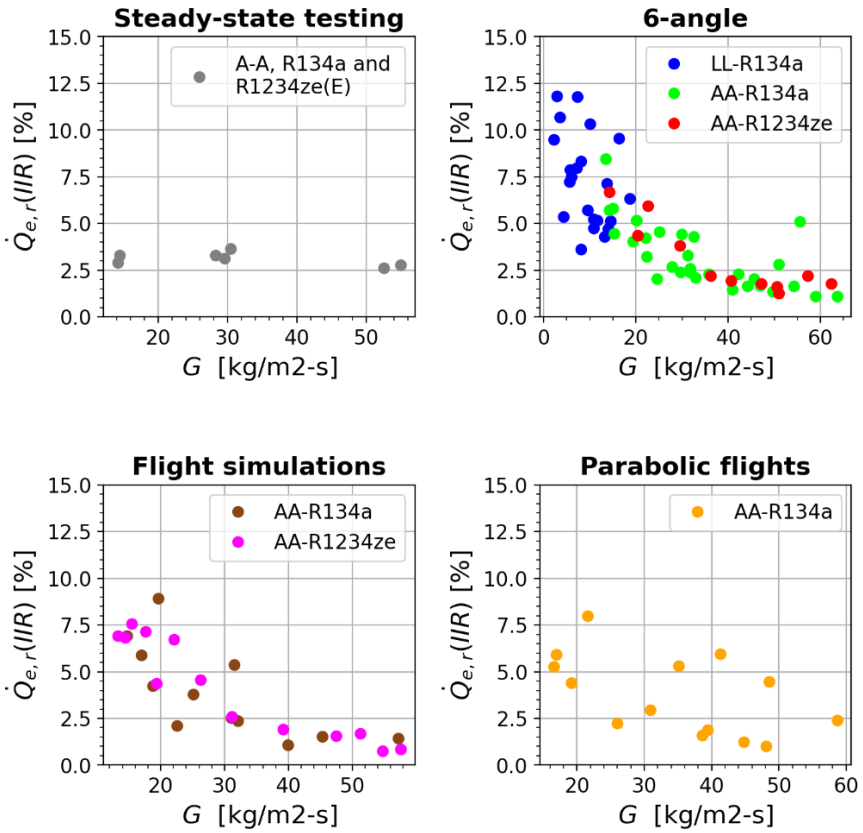

Figure 4: IIR of refrigerant side evaporator heat transfer rate for all datasets.

4.2 MMX(/AVG)

Figure 5 shows the MMX for evaporation and condensation temperatures as well as the MMX/AVG for the refrigerant side and air side heat transfer rates. All seven datasets are overlaid for each subplot.

Temperatures
Overall, the MMX of the evaporation temperature decreased with an increasing mass flux across all datasets. While the minimum of 1 K is negligible for most applications, a change of 10 K is very large. Looking at each dataset, it was noted that red, brown, magenta, and gray have very clear correlations with the mass flux within the datasets. For blue and green, the data points were more scattered and not as clearly correlated to the mass flux.

The condensation temperature showed very different patterns. For all datasets from the air-to-air configuration, the condensation temperature varied by no more than 2 K with the exception of a small number of data points varying by up to 3 K. In contrast, the condensation temperature of the liquid-to-liquid configuration varied within a band of up to 7 K. Strong correlations with the mass flux cannot be recognized.

Heat transfer rates

For the refrigerant side heat transfer (Figure 5 bottom left), the MMX/AVG of all inclination testing datasets with the air-to-air configuration formed a very similar trend (gray, green, red, brown, magenta). Even the steady-state results, which were constant for the IIR, followed a decreasing curve towards higher mass fluxes. Results for the liquid-to-liquid configuration fit into the trend but did not form a clear correlation by themselves. The parabolic flight data showed a linear decrease towards lower mass fluxes and were below the highest MMX/AVG values from inclination changes for a given mass flux.

For the heat source heat transfer rate (Figure 5 bottom right), the MMX/AVG was generally lower for all air-to-air configuration datasets than when the quantifier was calculated for the refrigerant side. This may be due to a slower response of the air-side than the refrigerant side, for example due to the thermal mass of the heat exchanger. Still, the parabolic flight data resulted in smaller MMX/AVG values than for the other datasets. The very large values of the MMX/AVG for the water-side (Figure 5, bottom right plot, blue dots) may have been the result of changes in the *water* flow rate due to inclination changes, which then would not be a representative measure for the instabilities of a typical refrigeration cycle.

General

Throughout all subplots in Figure 5, the liquid-to-liquid configuration always produced the highest instabilities. It cannot be determined whether this was dictated by the heat exchanger shape or the low refrigerant mass fluxes. Another general finding is that the parabolic flights showed relatively low MMX and MMX/AVG values for the evaporation temperature, the refrigerant side heat transfer rate, and the heat source heat transfer rate. The condensation temperature is an exception, where the parabolic flight maneuvers generally led to stronger MMX values than the inclination changes in the other air-to-air datasets. This is likely because the microgravity periods directly changed the flow regime and thereby the heat transfer mechanism (Brendel et al., 2022b), while for inclination changes the condensation temperature changed due to increased or decreased mass flow rates imposed by changes on the low pressure side of the cycle.

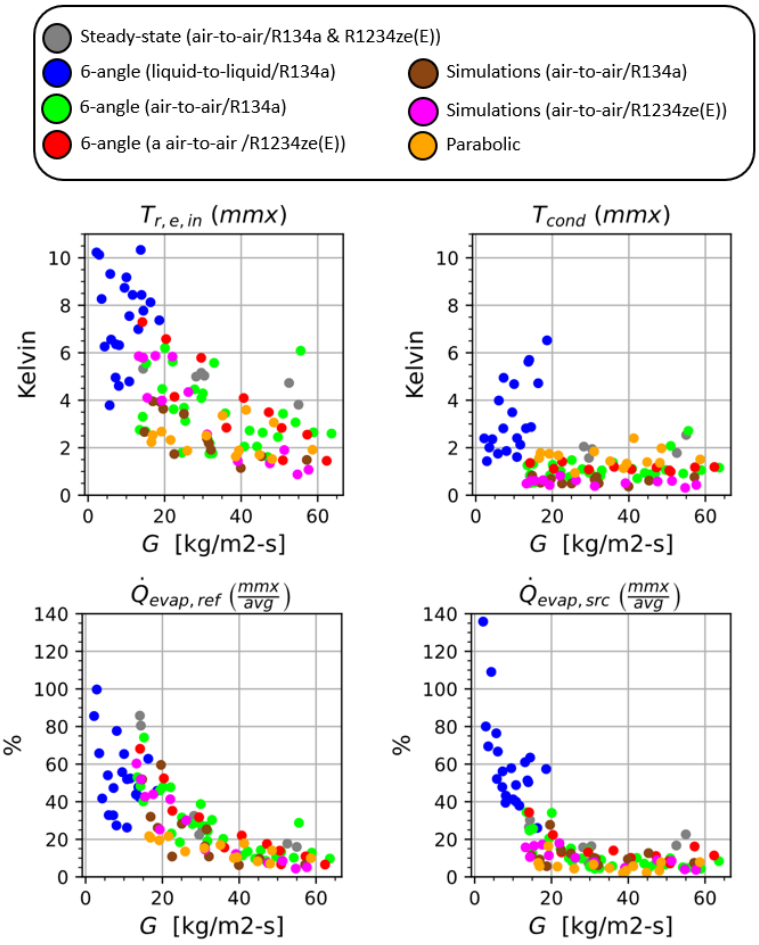

Figure 5: MMX and MMX/AVG quantifier for all testing series.

5. DISCUSSION

Quantifying instabilities of a vapor compression cycle induced by gravity perturbations is a wide-open research field. Quantifiers were proposed in this paper as MDV, IIR, MMX, 80%, MMX/AVG and 80%/AVG, but many other propositions characterizing the system response could be made and potentially be specified for certain applications (electronics cooling, air conditioning, coolers for biological samples) or certain vehicles (trucks, ships, orbital spacecraft, lunar lander).

For some applications, only the final state after a gravity perturbation may matter, while the transient behavior during the perturbation(s) is not of interest. Then, the proposed quantifier definitions are not applicable. Instead, one could simply declare a quantifier IME (initial minus end state), for which measurements at points 1 and 7 in Figure 3 are subtracted.

As a common limitation, the quantifiers are only meaningful if the cycle was at steady-state when the gravity perturbation started. If the cycle was in a transient state initially, then the MDV will naturally grow as the operating point of the cycle moves away from the initial state, even without any gravity perturbation. Similarly, the MMX and the IME grow without gravity perturbations if the initial state is transient.

A candidate quantifier for transient processes would be the DMA (deviation from a moving average). Figure 6 exemplifies this with hypothetical data shown in black. In this scenario, a property is measured to increase from 0 to 120 over a 2-minute period of time, but with a strong spike after 1 minute and 10 seconds. The IIR and MMX would be meaningless for this response because their result would not be dictated by the spike in the measurement. Plotting a 7 second moving average along the measurement (red line) shows a slight deviation for the smooth transient process but large deviation during the spike. The deviation is plotted in blue. The behavior of the blue line identified the spike and also quantifies it by the height of its own spike. However, such a quantifier requires additional research on the time window for the moving average and its utility when being adopted for varying gravity perturbation patterns. Such work is beyond the scope of this paper but would be an interesting topic for further research.

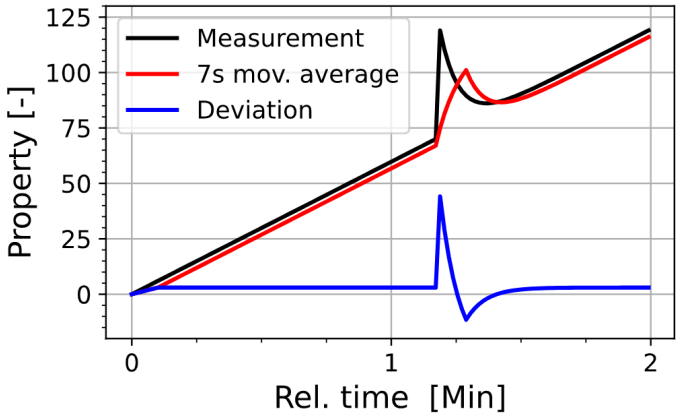

Figure 6: Visualization of DMA quantifier.

6. CONCLUSIONS

Seven different datasets were accumulated on a VCC experimental test stand, differentiated by the type of gravity perturbation, the refrigerant employed and the heat exchanger types leveraged. The datasets were evaluated in conjunction with proposed quantifiers useful to characterize instabilities induced by gravity perturbations. The main proposed quantifiers are the IIR for the mean deviation of any measurement from the initial steady-state and the MMX and the MMX/AVG for the maximum range of measurements due to a gravity perturbation.

Given *frequent* gravity perturbations, the IIR-quantifier proved that the vapor compression cycle is more gravity resilient at higher mass fluxes. For *infrequent* gravity perturbations, once every 15 to 20 minutes, a constant gravity dependence value of approximately 3% was found for mass fluxes from 14 to 58 kg/m²·s.

The MMX showed enhanced cycle stabilities as a function of higher mass fluxes for almost all datasets for heat transfer rates and the evaporation temperature. The MMX of the condensation temperature appeared to be a stronger function of the heat exchanger type than the gravity perturbation approach or mass flux.

Parabolic flight maneuvers caused generally smaller instabilities than those resulting from various ground-based inclination patterns. The only exception was the condensation temperature for the air-to-air configuration, where the parabolic flights caused higher instabilities than other gravity perturbations. For the given test stand, inclination testing is therefore a conservative estimate for instabilities to be expected on parabolic flights.

Searching for a quantifier that is applicable to cycles starting with a transient operation is proposed as useful future work. The deviation of a moving average was discussed as a candidate quantifier for said transient operations.

NOMENCLATURE

Symbols and acronyms

$AVG\ or\ avg$	Average value of transient data
DMA	Deviation of moving average
IIR	Inclination impact ratio
$INI\ or\ ini$	Initial value of test run
IME	Difference between initial and final value of transient data

Subscripts

$e\ or\ evap$	Evaporator
r	Refrigerant
src	(Heat) source
in	Inlet
$cond$	Condenser

MDV	Mean deviation		$e\ or\ evap$	Evaporator
MMX	Difference between maximum and minimum measured value			
$\dot{Q}$	Heat transfer rate	W		
T	Temperature	K		

ACKNOWLEDGEMENTS

The authors greatly appreciate the financial support by Air Squared, Inc. The support of this work by NASA under SBIR contract 80NSSC18C0049 is gratefully acknowledged. Mike Ewert and Stephen Caskey provided valuable guidance in the research and project management. Professor Justin Weibel's feedback was highly appreciated throughout the project, too.

REFERENCES

Azzolin, M., Bortolin, S., Le Nguyen, L.P., Lavieille, P., Glushchuk, A., Queeckers, P., Miscevic, M., Iorio, C.S., Del Col, D., 2018. Experimental investigation of in-tube condensation in microgravity. Int. Commun. Heat Mass Transf. 96, 69–79. https://doi.org/10.1016/j.icheatmasstransfer.2018.05.013

Brendel, L.P.M., 2021. Vapor Compression Refrigeration in Microgravity (Dissertation). Purdue University, West Lafayette.

Brendel, L.P.M., Caskey, S.L., Braun, J.E., Groll, E.A., 2022a. Effect of Orientation on the Steady-State Performance of Vapor Compression Cycles. Appl. Therm. Eng.

Brendel, L.P.M., Caskey, S.L., Braun, J.E., Groll, E.A., 2022b. Vapor compression refrigeration testing on parabolic flights: Part 2 - Heat exchanger performance. Int. J. Refrig.

Brendel, Leon P M, Caskey, S.L., Braun, J.E., Groll, E.A., 2021a. Similarity of Two-phase Cycle Stability Between Ground-Based Inclination and Parabolic Flight Experiments, in: Thermal & Fluids Analysis Workshop (TFAWS) 2021. Virtual.

Brendel, Leon P M, Caskey, S.L., Braun, J.E., Groll, E.A., 2021b. Stability Against Orientation Changes of a Vapor Compression Cycle in Two Configurations, in: DKV Meeting 2021. Dresden, p. 9.

Brendel, Leon P. M., Caskey, S.L., Ewert, M.K., Hengeveld, D., Braun, J.E., Groll, E.A., 2021. Review of vapor compression refrigeration in microgravity environments. Int. J. Refrig. 123, 169–179. https://doi.org/10.1016/j.ijrefrig.2020.10.006

Chiaramonte, F.P., Joshi, J.A., 2004. Workshop on critical issues in microgravity fluids, transport, and reaction processes in advanced human support technology (Workshop Final Report No. NASA/TM-2004-212940).

Domitrovic, R.E., Chen, F.C., Mei, V.C., Spezia, A.L., 2003. Microgravity heat pump for space station thermal management. Habitat. Elmsford N 9, 79–88.

Ginwala, K., 1961. Engineering study of vapor cycle cooling equipment for zero-gravity environment (Technical report No. TR 60-776). Wright-Patterson Air Force Base, Dayton, OH, USA.

Grzyll, L.R., Cole, G.S., 2000. A Prototype Oil-Less Compressor for the International Space Station Refrigerated Centrifuge. Presented at the International Compressor Engineering Conference, Purdue e-Pubs, West Lafayette, Indiana.

Hye, A., 1985. Use of two-phase flow heat transfer method in spacecraft thermal system, in: 20th Thermophysics Conference. Presented at the 20th Thermophysics Conference, American Institute of Aeronautics and Astronautics, Williamsburg, VA, U.S.A. https://doi.org/10.2514/6.1985-1050

Iceri, D.M., Zummo, G., Saraceno, L., Ribatski, G., 2020. Convective boiling heat transfer under microgravity and hypergravity conditions. Int. J. Heat Mass Transf. 153, 119614. https://doi.org/10.1016/j.ijheatmasstransfer.2020.119614

Narcy, M., 2014. Flow boiling in straight heated tube under normal gravity and microgravity conditions (Doctoral). University of Toulouse, Toulouse.

Rohleder, C.S., Bansal, K., Shaffer, B., Groll, E.A., 2018. Vapor Compression Refrigeration System for Cold Storage on Spacecrafts. Presented at the International Refrigeration and Air Conditioning Conference, Purdue e-Pubs.

Sunada, E., Miller, J., Ganapathi, G.B., Birur, G., Park, C., 2008. Start-Up Characteristics and Gravity Effects on a Medium/High-Lift Heat Pump using Advanced Hybrid Loop Technology, in: 38th SAE International Conference on Environmental Systems. https://doi.org/10.4271/2008-01-1959